J. Fluid Mech. (1992), *vol.* 236, *pp.* 461–476
Printed in Great Britain

The oblique ascent of a viscous vortex pair toward a free surface

By HANS J. LUGT AND SAMUEL OHRING
David Taylor Research Center, Bethesda, MD 20084-5000, USA

(Received 3 April 1991 and in revised form 30 August 1991)

The problem of a vortex pair, rising obliquely at an angle of 45° toward a deformable free surface in a viscous, incompressible fluid, is solved with the aid of the Navier–Stokes equations. The full nonlinear boundary conditions at the free surface are applied. The oblique interaction of the vortex pair with the free surface results in a number of novel features that have not been observed for the special case of a vertical rise, reported earlier. These features include the directional change of trajectories near the free surface and the occurrence of waves driven by the vortex pair. Moreover, surface tension can completely change the flow characteristics such as the direction of the trajectories and the generation of secondary vortices. Numerical solutions are presented for selected Reynolds, Froude, and Weber numbers.

1. Introduction

This investigation is a continuation, complement, and conclusion of two previous studies by Ohring & Lugt (1989, 1991, referred to as I and II in the following text), on two counter-rotating vortices of equal strength (vortex pair) approaching a deformable free surface. The purpose of this paper is twofold: to give information on the oblique interaction of a viscous vortex pair with a deformable free surface with all its implications in two-dimensional motion, and to be a precursor of a three-dimensional flow study, planned as a follow-up.

Vortex pairs, their generation and interaction with boundaries and other vortices, have recently become of interest in two main areas: in the study of wave signatures caused by ship wakes (Sarpkaya & Henderson 1984; Willmarth *et al.* 1989), and in the study of two-dimensional vortex dynamics. In the first area of ship hydrodynamics, two-dimensional vortex pairs have been used to simulate almost parallel vortex filaments behind ships or ship models. These filaments are subject to three-dimensional disturbances and develop to complex three-dimensional vortex configurations. Two-dimensional laminar vortex pairs can provide, at best, information on basic flow characteristics. However, since little is known about general vortex/free-surface interaction, such two-dimensional flow studies are of great value in understanding essential flow phenomena. In the second area, stratified flows and fluid motions under the influence of external forces, such as magnetic fields and rotation, tend to behave two-dimensionally. Here, vortex pairs play a vital role in the understanding of two-dimensional coherent flow patterns, in particular of turbulent structures (Couder & Basdevant 1986; Nguyen Duc & Sommeria 1988; Dritschel 1989; van Heijst & Flor 1989).

The vertical approach of a vortex pair toward a free surface has been studied extensively, and a brief summary of the literature is given in II. However, there is

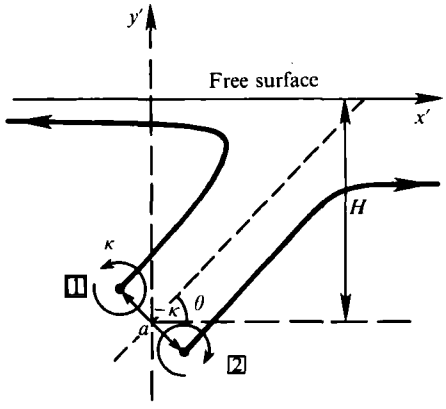

FIGURE 1. Sketch of the flow situation. The dimensional coordinates x', y' are related to the dimensionless ones by x', $y' = ax$, ay. The trajectories of the two vortices are solutions of the potential-flow problem with a flat surface.

little information on the oblique rise of a vortex pair. Acton (1976) gave a detailed account of the potential-flow solution in which two point vortices approach a surface. This solution must be obtained numerically and is given in figure 1 for the inclination angle $\theta = 45°$ as a benchmark. Ersoy & Walker (1986) studied the oblique approach of a vortex pair to a non-slip wall. They used an inviscid-flow model with a laminar boundary layer. The vortex closer to the wall generates a boundary layer, from which a secondary vortex develops. Between primary and secondary vortices an 'explosive boundary-layer growth' takes place in the form of a jet perpendicular to the wall. This phenomenon has been indicated in experimental observations by Harvey & Perry (1971).

More information is available for the similar problem of a vortex ring approaching a surface in an oblique way. This vortex-ring problem has relevance to the present study since any circular vortex ring, approaching a surface at an arbitrary inclination angle θ, possesses a symmetry plane defined by the translational velocity vector and the angle θ. Figure 1 then can be interpreted as showing such a symmetry plane. In contrast to a two-dimensional filament, however, a vortex ring stretches near a boundary and may become unstable or may reconnect. In what follows more details of the vortex-ring problem will be given.

Experiments by Kwon (1989) and Bernal & Kwon (1989) show that a laminar vortex ring approaching a water surface obliquely interacts with the surface in two different ways: the upper part of the ring breaks open near the surface and its ends attach to the surface ('reconnection process'), whereas the lower part either behaves like a straight piece of filament, producing a secondary vortex filament, or the lower part also reconnects at the free surface, forming a second half-ring. If both half-rings reconnect at the free surface, they either propagate away from each other or move parallel to each other. This latter behaviour is of particular interest in this study, because it can be investigated with a two-dimensional flow model. Experiments by Lim (1989) with vortex rings that approach a solid wall obliquely, do not reveal a break-up but show helical disturbances in the half-ring closer to the wall.

Numerical computations for axisymmetric vortex rings and filaments near a free surface were made by Dommermuth & Yue (1990) with the aid of the Navier–Stokes equations. Linearized free-surface boundary conditions were used, and the problem of the reconnection process of a vortex filament at the free surface was addressed.

2. Definition of the flow problem

Two counter-rotating vortices of equal strength κ, a distance a apart, rise obliquely through self-induction to an initially undisturbed free surface. The fluid is assumed to be incompressible, homogeneous, and Newtonian. The laminar flow problem is a transient one, with the fluid coming to rest after an infinitely long time. The initially undisturbed free surface is placed at $y = 0$ in a Cartesian coordinate system x, y (figure 1). The corresponding velocity components are u and v, respectively. At the initial depth H, where the vortex pair is placed, the translational velocity of the pair is V_0, which can be expressed by κ through $V_0 = \kappa/a$ (κ is related to the circulation Γ by $\kappa = \Gamma/2\pi$). The basic equations of motion are made dimensionless by the characteristic length a, the time a/V_0, and the velocity V_0. The pressure is made dimensionless by the stagnation pressure, and gravity is included so that the pressure equals $\rho V_0^2(P - y/Fr^2)$ with ρ the density of the fluid; P is the dimensionless dynamic pressure. In addition to the dimensionless depth $\delta = H/a$, the flow parameters are the Froude number $Fr = V_0/(ga)^{\frac{1}{2}} = \kappa/(ga^3)^{\frac{1}{2}}$, the Reynolds number $Re = V_0 a/\nu = \kappa/\nu$, and the Weber number $We = \sigma a/\rho\kappa^2$, where ν and g are the kinematic viscosity of the fluid and the constant of gravity, respectively. The coefficient of surface tension σ is considered a constant.

The initial-boundary-value problem is described by

$$u_t + (u^2)_x + (uv)_y = -P_x + \frac{1}{Re}(u_{xx} + u_{yy}), \tag{1}$$

$$v_t + (uv)_x + (v^2)_y = -P_y + \frac{1}{Re}(v_{xx} + v_{yy}), \tag{2}$$

$$u_x + v_y = 0, \tag{3}$$

with t the dimensionless time. The free surface is given by $y = Y(x, t)$ and is part of the solution. For the oblique rise the remaining semi-infinite domain is made finite for numerical calculations by the boundaries $x = x_{L1}$, x_{L2} and $y = y_L$. Then, the boundary conditions are

$y = Y$:

$$Y_t = v - uY_x, \tag{4}$$

$$\left(P - \frac{Y}{Fr^2} - \frac{2}{Re}u_x\right)Y_x + \frac{1}{Re}(u_y + v_x) = -We\frac{Y_{xx}}{(1+Y_x^2)^{\frac{3}{2}}}Y_x, \tag{5}$$

$$\left(P - \frac{Y}{Fr^2} - \frac{2}{Re}v_y\right) + \frac{1}{Re}(u_y + v_x)Y_x = -We\frac{Y_{xx}}{(1+Y_x^2)^{\frac{3}{2}}}. \tag{6}$$

$y = y_L$: $P = 0$, u, v: obtained by second-order extrapolation along a coordinate line into the interior, (7)

$x = x_{L1}$, x_{L2}, $y_L < y \leqslant 0$:

$P = 0$, u, v: obtained by second-order extrapolation along a coordinate line into the interior. (8)

The following assumptions are made for the initial conditions at $t = 0$: two point vortices 1 and 2 of strengths $\pm\kappa$ are introduced at the positions $(x_v, y_v)_1 =$

$(-\frac{1}{4}\sqrt{2}, \delta+\frac{1}{4}\sqrt{2})$ and $(x_v, y_v)_2 = (+\frac{1}{4}\sqrt{2}, \delta-\frac{1}{4}\sqrt{2})$. The induced flow field is irrotational except in the vicinity of the vortex centres. This circular vicinity with radius r_L is described by the Lamb formula for the decaying potential vortex:

$$v_\varphi = -\frac{1}{r}\left[1-\exp\left(-\frac{r^2 Re}{4t_L}\right)\right], \quad r \leqslant r_L. \tag{9}$$

with $v_\varphi = (u^2+v^2)^{\frac{1}{2}}$ and $r^2 = (x-x_v)^2+(y-y_v)^2$. The error of using (9), defined by the amount of vorticity at $r = r_L$, as a percentage of the maximum core vorticity at $r = 0$, is less than 0.2% for $t_L = 0.25$ at $r_L = \frac{1}{4}$. The numerical computation starts at $t = 0$.

The trajectories of two point vortices that approach a flat surface obliquely in a potential-flow environment are computed as reference curves. According to Acton (1976), only the following two ordinary differential equations are required to determine those trajectories:

$$\frac{dx_2}{dt} = \frac{c}{X^2+c^2}+\frac{2y_2+c}{X^2+(2y_2+c)^2}-\frac{1}{2y_2}, \tag{10}$$

$$\frac{dy_2}{dt} = X\left[\frac{1}{X^2+c^2}-\frac{1}{X^2+(2y_2+c)^2}\right], \tag{11}$$

because of the two existing integrals of motion

$$X(t) = \left[\frac{4y_2(y_2+c)c^2-(2y_2+c)^2}{1-4y_2(y_2+c)}\right]^{\frac{1}{2}}, \tag{12}$$

$$y_1(t) = y_2+c, \tag{13}$$

in the half-plane $y \leqslant 0$ with $X = x_2-x_1$. The set of equations (10) and (11) was solved by a Runge–Kutta method. For the inclination angle of 45°, $c = \cos 45°$, and the curves are shown in figures 1 and 4(*a*). Since the trajectories of the two vortices do not start at infinity, there is a minute tilting which is neglected because it is irrelevant to this study. For $|x| \to \infty$ it follows from (12) that

$$4y_1 y_2 = 1, \tag{14}$$

a relation which is satisfied by the curves in figures 1 and 4(*a*).

3. Remarks on the numerical procedure

Since the numerical technique for solving the initial-boundary-value problem is described in I, only an outline with additional features pertinent to the new, oblique flow situation is given here. Obviously, the total flow field must now be considered, rather than only one-half of it as required in the symmetric vertical rise of a vortex pair. For all cases computed in this paper, the flow region extends from $x_{L1} = -8.34$ to $x_{L2} = 13.3$ and from $y_L = -6.0$ to the free surface and is represented by 433×203 points; but only a section of the whole flow domain is shown in the figures that follow. The number of time steps is of the order of 10^5.

For the numerical solution of the initial-boundary-value problem, defined by (1)–(9), it is convenient to make a boundary-fitted coordinate transformation. The coordinate lines in physical space are mapped onto a uniformly spaced Cartesian mesh with a unit mesh spacing in each coordinate direction. As the flow field evolves

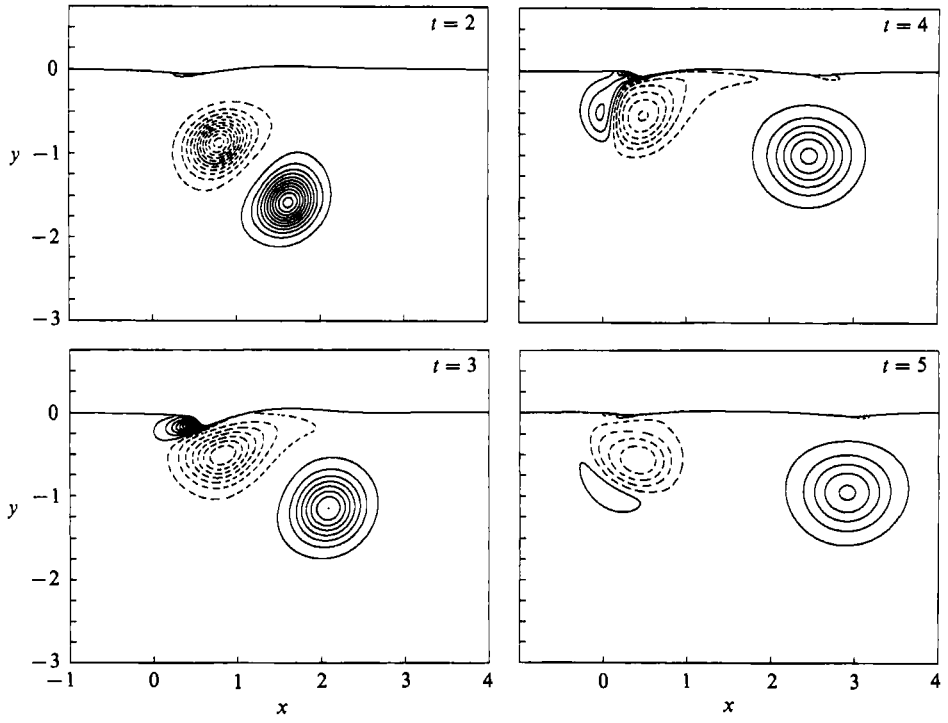

FIGURE 2. Equivorticity lines for $Re = 100$, $Fr = 0.2$, $We = 0$ at four different times. The ω-contours are $\ldots -3, -1, +1, +3, \ldots$.

in time, the grid in physical space will move and its coordinate lines will be attracted to regions of high flow gradients through the use of an adaptive-grid technique. However, the Cartesian grid in computational space always remains fixed and uniform. This is the major advantage of using a mapping.

The continuity equation (3) is replaced by an equation with pseudo-compressibility for numerically conserving mass at each physical time step:

$$P_\tau + u_x + v_y = 0. \tag{15}$$

τ is the pseudo-time. In this technique, pseudo-time steps are required to satisfy the continuity equation (3) at each new physical time step Δt. Spatially varying pseudo-time steps that depend on mesh-cell size are used (see I). Typically two to five pseudo-time steps are needed per physical time step, their number decreasing with smaller physical time steps. Mass conservation was excellent for all cases computed.

Five partial differential equations for u, v, x, y, and P must be solved with the proper boundary conditions. The finite-difference technique for solving these equations is briefly described in the following way. All spatial derivatives, including one-sided derivatives at the boundaries, are replaced by finite-difference operators of second order in the computational space. The time-differencing procedure is implicit. The dynamic pressure field P at $t = 0$ is obtained by solving a Poisson equation for P in terms of the initial velocity field. This is the only time a Poisson equation for P is used. A 'four-colour' scheme is used in the interior of the computational space. The use of such a scheme, which can be vectorized, resulted in an order of magnitude increase in computer speed on the Cray-XMP 24 on which the computations were performed.

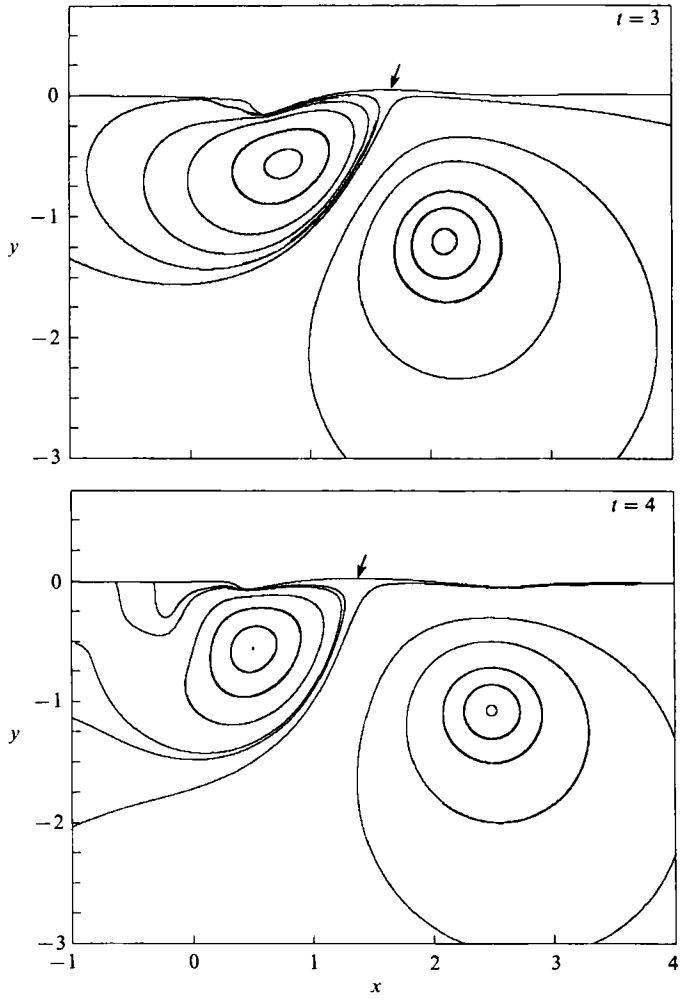

FIGURE 3. Streamlines for $Re = 100$, $Fr = 0.2$, $We = 0$ at two different times. The arrows indicate stagnation points.

The computational cycle for one complete pseudo-time step iteration consists of (*a*) applying the 'four-colour' scheme to compute updates for x and y; (*b*) applying the 'four-colour' scheme to compute updates for u, v, and P; (*c*) obtaining updates for u and v from (8) at successive points along the boundary $x = x_{L1}$; (*d*) obtaining updates for P, u, v, and Y at successive points along the free surface; and (*e*) obtaining updates for u and v from (8) at successive points along the boundary $x = x_{L2}$ and then along the boundary $y = y_L$ from (7).

At the completion of this computational cycle, after the latest updates for x, y, u, and v satisfy certain convergence criteria at all points, these updates are the solution at the new time level $n+1$. If the convergence criteria are not met, cycle (*a*)–(*e*) is repeated until they are met. The accuracy of the numerical scheme was checked with fine grids in I. For the case $Fr = 0.4$, $We = 1$, wave reflection at the outer boundary $x = x_{L2}$ was first observed at $t = 8.50$, at which time the computation was stopped. Reflection did not yet occur in the other cases.

Streamline pictures show only selected streamlines obtained numerically from the velocity fields since the stream function was not computed in this paper. This means

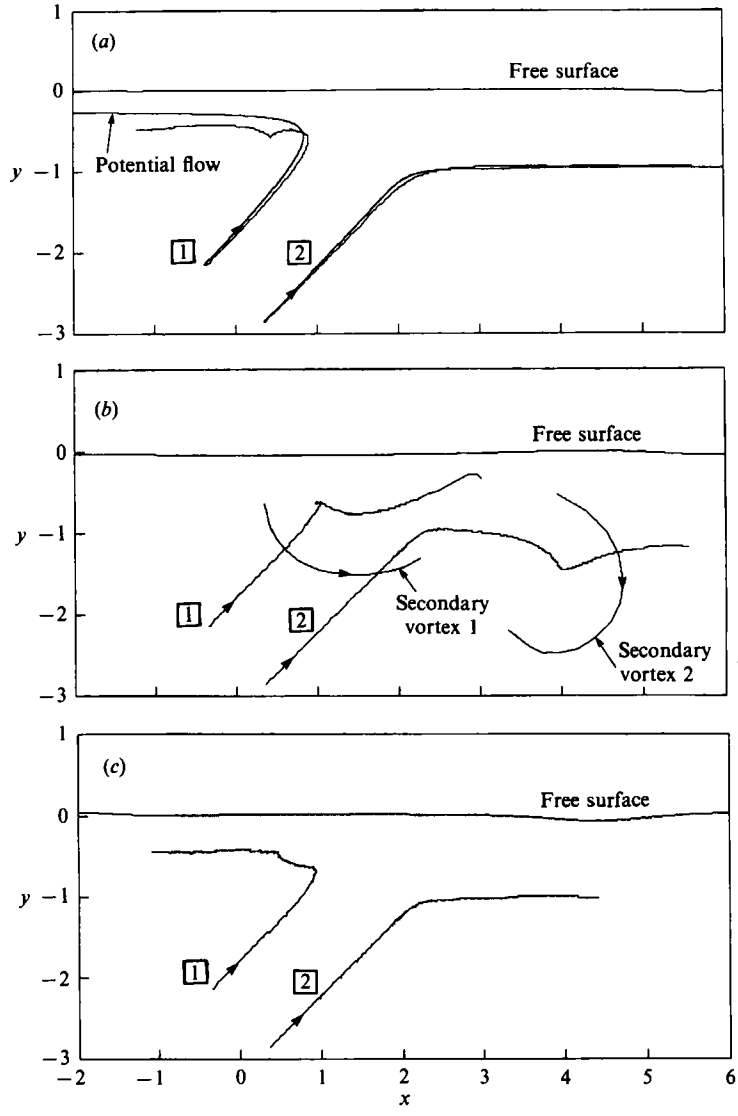

FIGURE 4. (*a*) Paths of the vortex centres for $Re = 100$, $Fr = 0.2$, $We = 0$. For comparison, the potential-flow solution for a flat surface is included. The free surface is plotted for the final time $t = 11.02$. (*b*) Paths of the centres of the primary and secondary vortices for $Re = 100$, $Fr = 0.4$, $We = 0$. The free surface is plotted for the final time $t = 17.0$. (*c*) Paths of the vortex centres for $Re = 100$, $Fr = 0.4$, $We = 1$. The free surface is plotted for the final time $t = 8.50$.

that the streamlines selected do not represent equally incremental values of the mass flux and that they must be interpreted with caution.

4. Results

Following the selection of flow parameters in II, four different cases, all for $Re = 100$, have been computed: $Fr = 0.2$, 0.4, 0.8 with $We = 0$ and $Fr = 0.4$ with $We = 1$. The flow field for $Fr = 0.2$ shows the least surface deformation. Equivorticity lines and streamlines are plotted in figures 2 and 3, respectively. The interaction of the vortices with the free surface is very similar to that of the vortices in the vertical

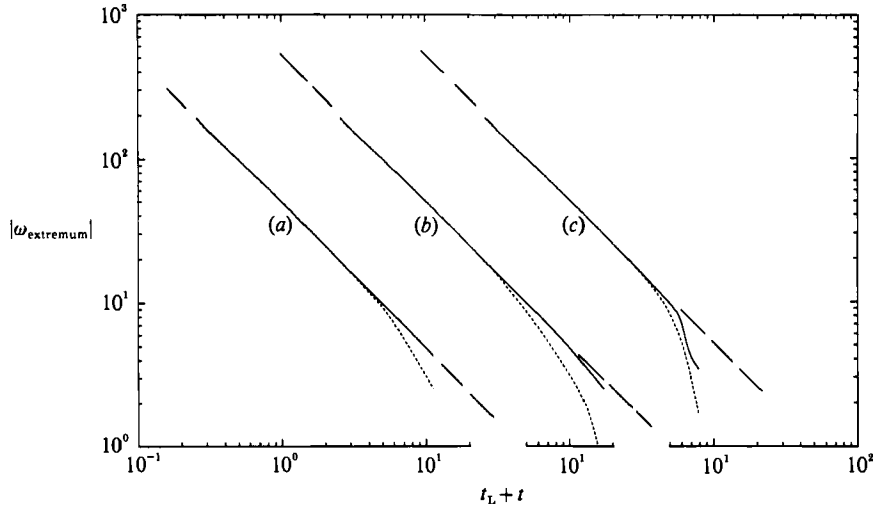

FIGURE 5. Decrease of $|\omega_{\text{extremum}}|$ with time for the primary vortices at all cases. Dotted lines represent vortex 1 and solid lines vortex 2. Dashed lines represent equation (16). Curve (*a*) represents $Fr = 0.2$, $We = 0$ and $Fr = 0.4$, $We = 1$; curve (*b*) $Fr = 0.4$, $We = 0$; and curve (*c*) $Fr = 0.8$, $We = 0$.

ascent except that here vortex 1 reaches the surface first. The vortex generates a scar, to the left of which vorticity of opposite sign (negative vorticity) is created. The amount of vorticity generated is, for a fixed or almost fixed surface, twice the surface curvature times tangential surface velocity. The negative vorticity field becomes, when a local minimum in the vorticity field occurs, a secondary vortex which is shed into the flow interior. Meantime, vortex 2 has approached the free surface, but its strength has weakened and it is not able to produce a significant scar and a secondary vortex. The corresponding streamline patterns for $t = 3.0$ and 4.0 in figure 3 reveal an almost steady free surface with stagnation points between the two primary vortices indicated by arrows. The streamlines ending at the stagnation points (not drawn in figure 3) must always be perpendicular to the free surface in a steady flow (Lugt 1987). The two streamlines to the left at $t = 4.0$, ending at the free surface, are not stagnation streamlines but indicate a very weak movement of the free surface. This indication has been validated by additional computations not presented here.

The paths of the vortex centres are shown in figure 4(*a*). Vortex 2 follows quite closely the path obtained from the potential flow solution, whereas vortex 1 makes a sharper turn and stays farther away from the surface. As in the vertical approach, the decrease of $|\omega_{\text{extremum}}|$ at the vortex centre with time, shown in figure 5(*a*), follows a relation which is derived from Lamb's formula (9)

$$\frac{|\omega_{\text{extremum}}|}{Re} = \frac{1}{2(t_L+t)}, \tag{16}$$

as long as the vortex is not weakened by another vorticity field of opposite sign. A detailed discussion will follow below.

In II the most dramatic case is $Fr = 0.4$, $We = 0$ in the sense that the paths of the primary and secondary vortices form loops during the vertical rise. Here, in the oblique case, the result is unexpected too, although in a different way. Vortex 1 with positive vorticity reaches the free surface first and generates an elevation with a sharp scar to the left (figure 6). However, instead of continuing to the left as one

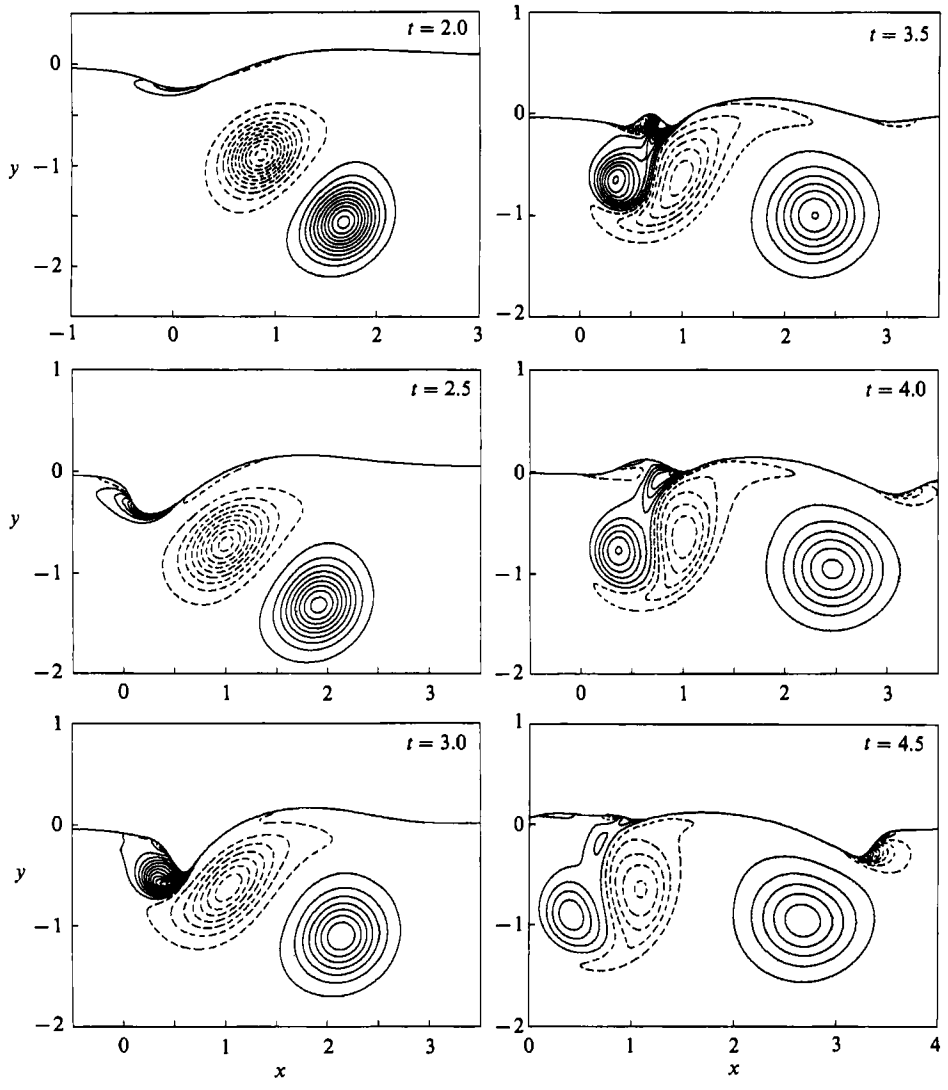

FIGURE 6. For caption see page 470.

would expect, the vortex lingers for a while and then moves to the right (figure 4*b*). The observation that the vortex pair can either separate near the surface or move together along the surface is reminiscent of the behaviour of vortex rings which, after reconnection to half-rings at the surface, either move away or keep together. During the time vortex 1 is trapped, it is stretched and turned.

In order to analyse this behaviour in more detail, the local flow around the vortex is approximated by a vortex in a shear flow. The corresponding inviscid-flow model was examined by Kida (1981) and Polvani & Wisdom (1990) for elliptic vortex patches (regions with uniform vorticity) and by Dritschel (1989) for non-uniform vortices. The major features of such a sheared vortex are rotation or oscillation of the elliptic region and 'stripping,' that is, the loss of weaker vorticity at the highest curvature of the elliptic vortex. Larger vorticity gradients at the vortex boundary develop with subsequent rounding of the vortex in a flow environment with less shearing. This behaviour is observed in figures 6 and 7. The elliptic deformation

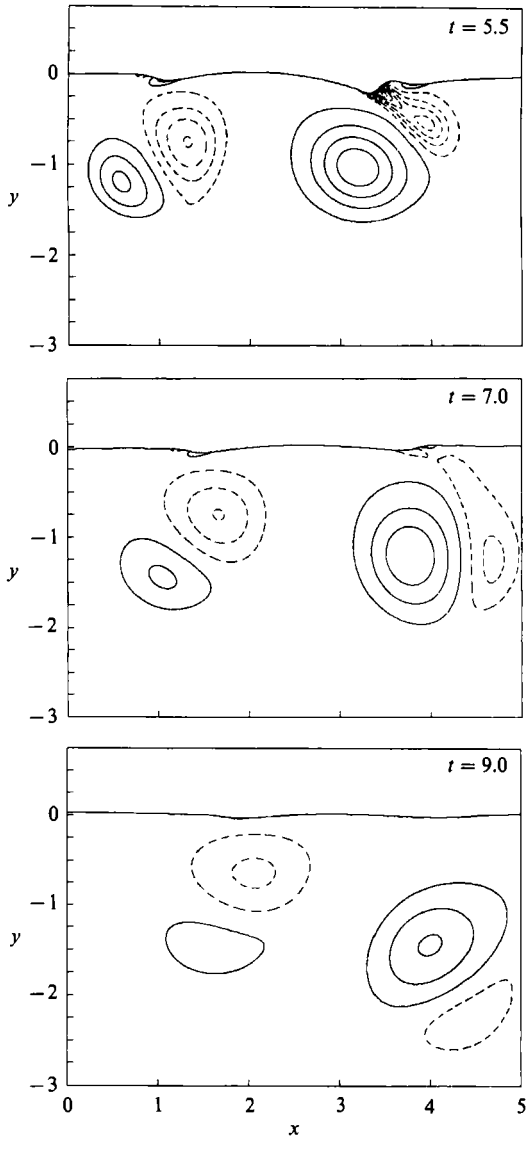

FIGURE 6. Equivorticity lines for $Re = 100$, $Fr = 0.4$, $We = 0$ at nine different times. The ω-contours are $\ldots -3, -1, +1, +3, \ldots$.

starts at about $t = 2.5$ with stripping and rotation taking place thereafter until $t \approx 5.0$. Vortex 1 weakens during this process, compared to vortex 2, and has about the same strength as the secondary vortex which it creates at the free surface. The decrease of $|\omega_{\text{extremum}}|$ with time for the primary vortices is shown in figure 5(*b*).

Both primary vortices produce during their ascent a steep hump of the free surface, vortex 1 at about $t = 3.5$ and vortex 2 at about $t = 5.5$. Such a hump was observed for the vertical rise too. The generation of positive and negative surface vorticity in a narrow local area at the scar causes a jet which pushes the surface up. The jet is clearly visible in the streamline picture for $t = 3.5$ in figure 7. Once the secondary vortex has been established, the newly created pair of vortices (consisting of the primary and the secondary vortices) moves downward through mutual

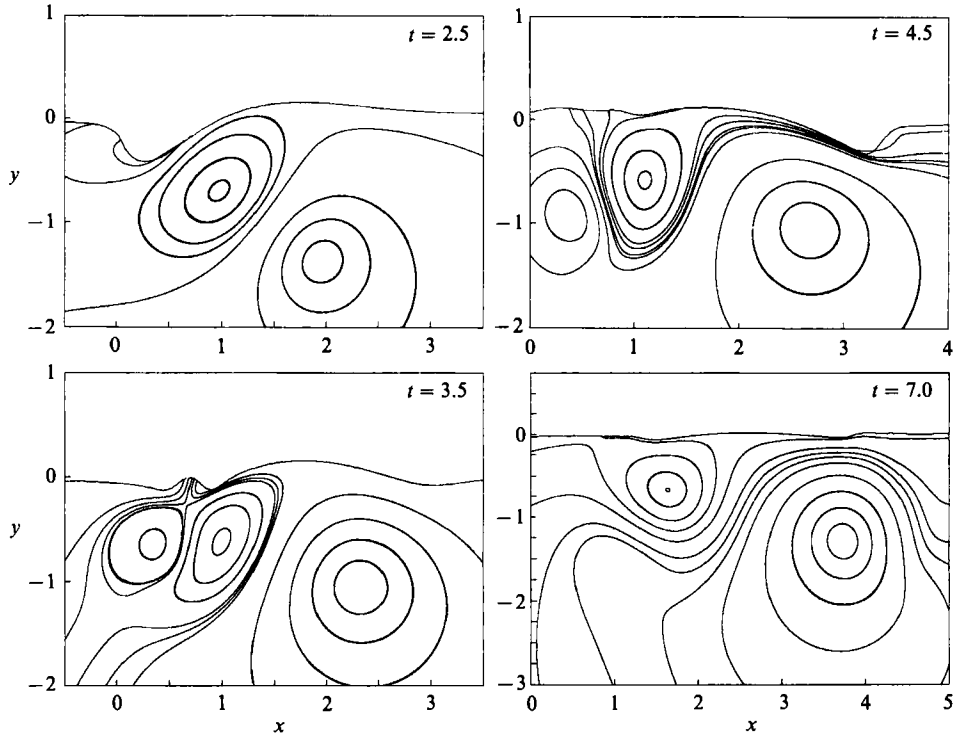

FIGURE 7. Streamlines for $Re = 100$, $Fr = 0.4$, $We = 0$ at four different times.

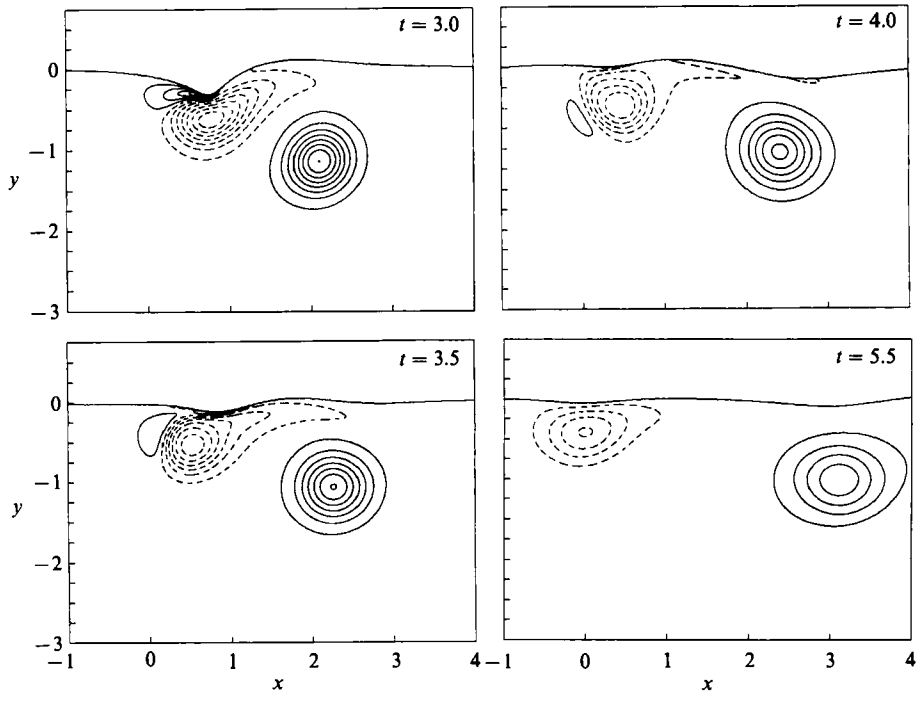

FIGURE 8. Equivorticity lines for $Re = 100$, $Fr = 0.4$, $We = 1$ at four different times. The ω-contours are $\ldots -3, -1, +1, +3, \ldots$.

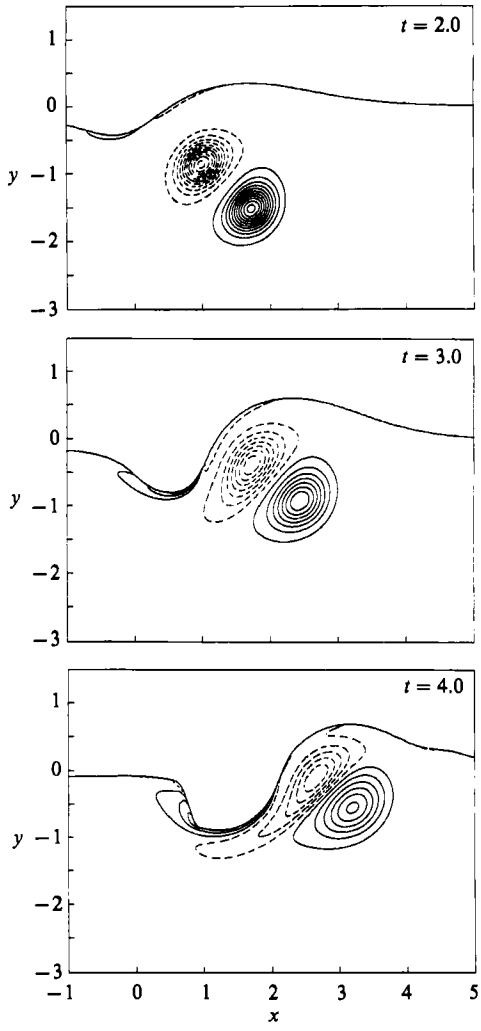

FIGURE 9. For caption see facing page.

induction. The hump of the free surface collapses. The local eruption of fluid close to the secondary vortex is a phenomenon similar to that of the 'explosive boundary layer' described for the oblique approach of a vortex pair to a non-slip wall by Ersoy & Walker (1986). In that case the direction of the fluid jet obviously is directed away from the wall, while both directions are possible at a free surface.

The influence of a constant coefficient of surface tension on the flow field is revealed in figures 4(*c*) and 8 for $Fr = 0.4$, $We = 1$. The difference between $We = 0$ and $We = 1$ is staggering. Flow fields and trajectories of the vortex pair are completely different owing to the smoothing of the free surface by the surface tension. In fact, there is quite a similarity to the case $Fr = 0.2$, $We = 0$ in figures 2 and 4(*a*) due to the weak surface deformation and complete agreement with figure 5(*a*) for the decrease of $|\omega_{\text{extremum}}|$ with time.

The flow field for $Fr = 0.8$, $We = 0$ exhibits the largest surface disturbance of the cases computed. The calculation of the corresponding situation for the vertical rise had to be terminated because of the steepness of the surface. The mushroom-like shape then indicated possible wave breaking. This is not the case in the 45° ascent.

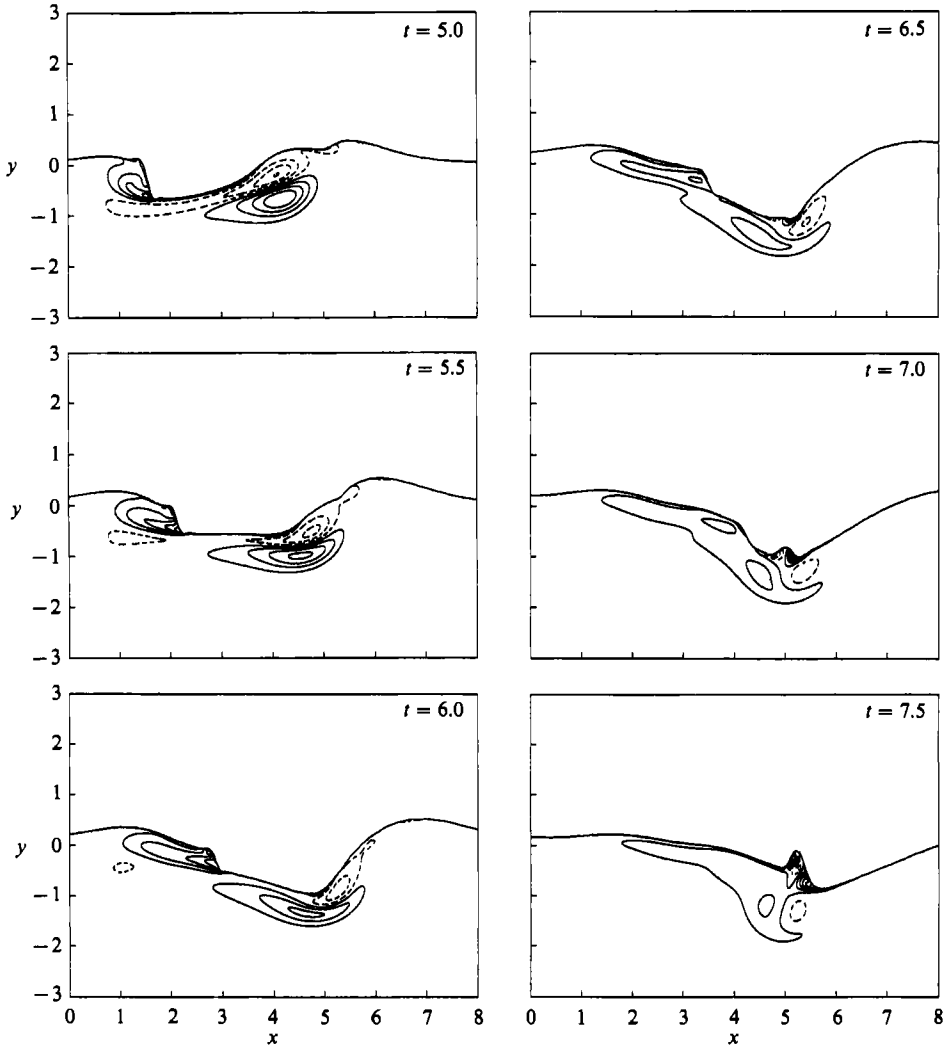

FIGURE 9. Equivorticity lines for $Re = 100$, $Fr = 0.8$, $We = 0$ at nine different times. The ω-contours are $\ldots -3, -1, +1, +3, \ldots$.

The computation could be carried out to the end desired. Equivorticity lines and streamlines are shown in figures 9 and 10, respectively. The vortex pair pushes the free surface up during its approach (figure 9, $t = 4.0$). Vortex 1, being closer to the surface and squeezed between the surface and vortex 2, pays its toll by getting stretched and sheared and in this process weakened ($t = 4.0$). Until about $t = 5.5$ the surface elevation is a wave, which consists of the vortex pair beneath, and which moves forward with the speed of the vortex pair. Beyond that time the wave crest travels on its own while the disintegrating vortex pair creates an irregular trough with even a small hump at $t = 7.0$. At $t = 7.5$ the trough is filling up, with a final upheaval in the form of a pronounced hump. The corresponding streamlines in figure 10 support this scenario. The direction of the surface movement is indicated by the angle of the streamlines at the surface. The trajectories in figure 11 show the joint movement of the vortex pair to the right. Rebound and final curling at $t \approx 7.5$ are caused by the passing of the surface trough.

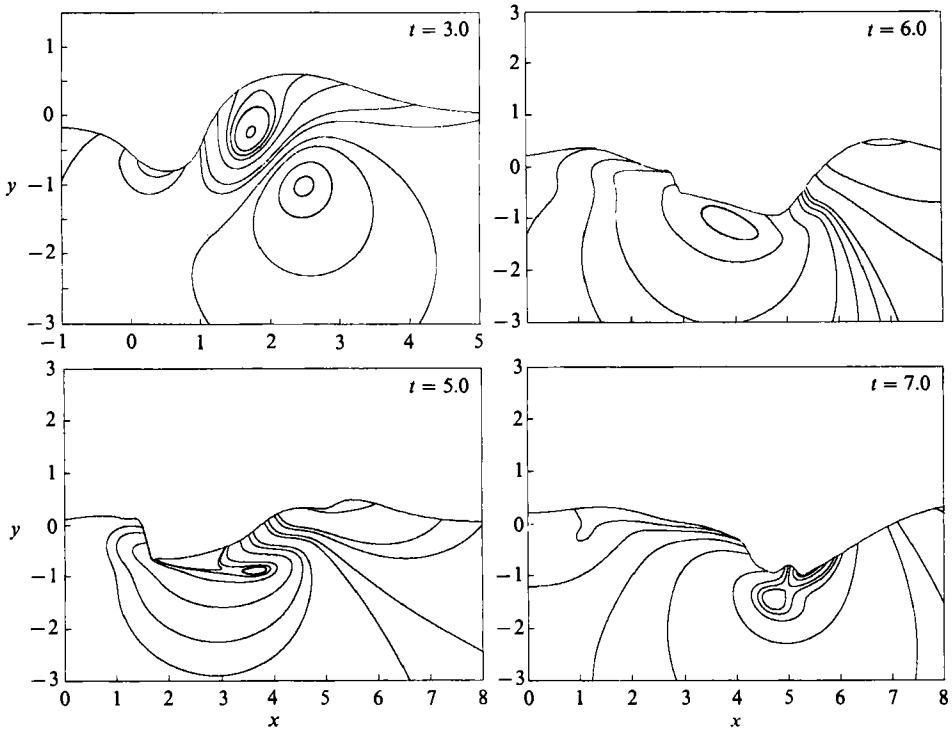

FIGURE 10. Streamlines for $Re = 100$, $Fr = 0.8$, $We = 0$ at four different times.

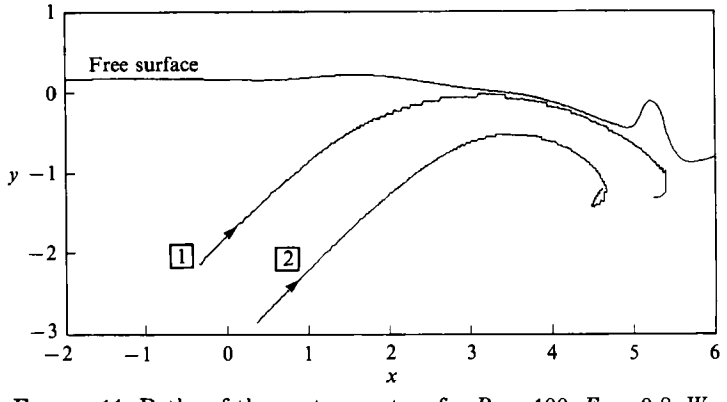

FIGURE 11. Paths of the vortex centres for $Re = 100$, $Fr = 0.8$, $We = 0$.
The free surface is plotted for the final time $t = 7.54$.

The decrease of $|\omega_{\text{extremum}}|$ with time is plotted in figure 5(*c*). The results for the other cases in figure 5 and for the vertical ascent in II, permit an assessment to be made of the validity of (16) and the subsequent deviation from it. As long as the vortices decay like a single vortex, Lamb's formula (16) holds. The encounter with another vorticity field of opposite sign, however, weakens the original vortex, and the decay accelerates. This happens in all cases of II for the vertical ascent with the initial depth of $\delta = 3.0$ at $t = 6$. In the oblique cases of this paper, the initial depth is $\delta = 2.5$ and vortex 1, which is closer to the free surface, weakens first from $t = 3$ on. The faster decay of vortex 2 starts at $t = 10$, except for $Fr = 0.8$, in which case the starting time is $t = 5$.

The weakening of a vortex by encounters with other vorticity fields of opposite sign, created by the free surface or/and by the presence of the partner vortex, may be compared with that from the merging of a vortex pair. This merging causes a deviation from (16) that was computed by Lo & Ting (1976). The deviation is very similar to those in figure 5. It is conjectured that the curve by Lo & Ting for a merging vortex pair approaches asymptotically the form $\sim 1/t^2$, since the leading term for the field with $\kappa_1 - \kappa_2 = 0$ is a decaying dipole. Further weakening by the surface as a source of opposite vorticity can happen as the steeper curve in figure 5(*c*) indicates.

The initial behaviour of the vortex pair as single vortices may also explain the good agreement of the trajectories with those of the potential-flow solution (figures 4*a* and 4*c*), provided the free surface is sufficiently flat. Since the circulation of the decaying vortices decribed by (9) remains constant with time, the vortices act beyond a certain distance like a potential vortex (Ting 1981). At a later time, when the various interacting forces are felt throughout the flow field, free surface and vortex patterns become surprisingly complex for such a low Reynolds number.

5. Conclusions

The interaction of a vortex pair with a deformable free surface in a viscous, incompressible, and homogeneous fluid results in flow phenomena which are intrinsic to viscous fluid properties. The ascending vortex pair causes elevations and indentations of the free surface (that in itself is an inviscid flow effect). Vorticity is created at the curved surface that is a prerequisite for the development of secondary vortices. They in turn can influence the trajectories of the primary vortices considerably. Not only rebounding has been observed but also complete loops performed by both primary and secondary vortices, which rotate around each other. Large vorticity gradients between primary and secondary vortices can occur that cause strong local upwelling of the surface, similar to boundary-layer ejection on a non-slip wall.

Reynolds-number effects, presented in II, are studied for $Re \leqslant 100$. Slow-motion behaviour is clearly evident for $Re = 10$, when the flow field is compared with that at $Re = 50$. The qualitative difference between $Re = 50$ and 100 is, in comparison, minor. The decay of the individual vortex follows (16) for a decaying potential vortex until vorticity from other sources interferes.

High and low Froude numbers represent the two extremes of free-surface yielding and stiffness, respectively. For $Fr = 0.8$ the vertically rising vortex pair generates a mushroom-like surface deformation which probably will lead to wave breaking. This is a conjecture because the actual wave breaking could not be computed. The 45°-oblique rise, on the other hand, could be investigated until virtual decay. These calculations revealed wave motions driven by the vortex pair beneath. For the low Froude number of 0.2 the free surface is barely deformed except for two local indentations called 'scars'. In the oblique case, the trajectory of vortex 2 deviates very little from that for potential flow, whereas the trajectory of vortex 1, which is closer to the surface, is influenced by secondary vortex 1.

The oblique rise of the vortex pair can cause special effects, not occurring in the vertical rise. The trajectories can change their direction owing to surface effects. A vortex may even linger at a place near the surface and may exhibit the rotating behaviour known from the Kida vortex ($Fr = 0.4$, $We = 0$).

Surface tension can influence the flow field considerably. It can change the

direction of the trajectories and can alter the generation process of secondary vortices because of surface levelling.

All computations are restricted to two-dimensional flows. Based on experimental evidence of three-dimensional effects, the question arises as to how long the two-dimensionality of the flow may remain, even for the flow cases which tend to behave two-dimensionally owing to external forces. Instability and three-dimensional effects may enforce a different picture, a conjecture that only future investigation will clarify.

This work was supported jointly by the DTRC Independent Research Program and by the Office of Naval Research, Fluid Dynamics Program, under Dr E. P. Rood.

REFERENCES

ACTON, E. 1976 The modelling of large eddies in a two-dimensional shear layer. *J. Fluid Mech.* **76**, 561–592.

BERNAL, L. P. & KWON, J. T. 1989 Vortex ring dynamics at a free surface. *Phys. Fluids* A **1**, 449–451.

COUDER, Y. & BASDEVANT, C. 1986 Experimental and numerical study of vortex couples in two-dimensional flows. *J. Fluid Mech.* **173**, 225–251.

DOMMERMUTH, D. G. & YUE, D. K. P. 1990 A numerical study of three-dimensional viscous interactions of vortices with a free surface. In *Eighteenth Symp. on Naval Hydrodynamics, The University of Michigan, Ann Arbor, Michigan*, pp. 1–61.

DRITSCHEL, D. G. 1989 Strain-induced vortex stripping. In *Mathematical Aspects of Vortex Dynamics* (ed. R. E. Caflish), pp. 107–119. SIAM.

ERSOY, S. & WALKER, J. D. A. 1986 Flow induced at a wall by a vortex pair. *AIAA J.* **24**, 1597–1605.

HARVEY, J. K. & PERRY, F. J. 1971 Flowfield produced by trailing vortices in the vicinity of the ground. *AIAA J.* **9**, 1659–1660.

HEIJST, G. J. F. VAN & FLOR, J. B. 1989 Laboratory experiments on dipole structures in a stratified fluid. In *Proc. 20th Int. Liege Colloq. on Ocean Hydrodynamics*, pp. 591–608. Elsevier.

KIDA, S. 1981 Motion of an elliptic vortex in a uniform shear flow. *J. Phys. Soc. Japan* **50**, 3517–3520.

KWON, J. T. 1989 Experimental study of vortex ring interaction with a free surface. Ph.D. thesis, University of Michigan.

LIM, T. T. 1989 An experimental study of a vortex ring interacting with an inclined wall. *Exps. Fluids* **7**, 453–463.

LO, R. K. C. & TING, L. 1976 Studies of the merging of vortices. *Phys. Fluids* **19**, 912–913.

LUGT, H. J. 1987 Local flow properties at a viscous free surface. *Phys. Fluids* **30**, 3647–3652.

NGUYEN DUC, J. & SOMMERIA, J. 1988 Experimental characterization of steady two-dimensional vortex couples. *J. Fluid Mech.* **192**, 175–192.

OHRING, S. & LUGT, H. J. 1989 Two counter-rotating vortices approaching a free surface in a viscous fluid. *David Taylor Research Center Rep.* DTRC-89/013 (referred to herein as I).

OHRING, S. & LUGT, H. J. 1991 Interaction of a viscous vortex pair with a free surface. *J. Fluid Mech.* **227**, 47–70 (referred to herein as II).

POLVANI, L. M. & WISDOM, J. 1990 On chaotic flow around the Kida vortex. In *Topological Fluid Mechanics* (ed. H. K. Moffatt & A. Tsinober), pp. 34–44. Cambridge University Press.

SARPKAYA, T. & HENDERSON, D. O. 1984 Surface disturbances due to trailing vortices. *Naval Postgraduate School Monterey, California, Rep.* NPS-69-84-004.

TING, L. 1981 Studies on the motion and decay of a vortex filament. In *Advances in Fluid Mechanics Conf. Aachen* Lecture Notes in Physics, vol. 148, pp. 67–105. Springer.

WILLMARTH, W. W., TRYGGVASON, G., HIRSA, A. & YU, D. 1989 Vortex pair generation and interaction with a free surface. *Phys. Fluids* A **1**, 170–172.